Supplemental Information:

Figure S1, Related to Figure 1. Generation of NDI1 knock-in mice and confirmation of NDUFS4 knock-out and NDI1 knock-in. **(A)** Schematic of the NDI1-LSL targeting construct for knock-in at the mouse *Rosa26* locus. Homologous recombination in embryonic stem cells after electroporation allows the generation of mice with the NDI1-LSL allele in their germline. Cre-mediated recombination of LoxP sites leads to deletion of the STOP cassette and expression of the yeast enzyme NADH Dehydrogenase Internal 1 (NDI1). **(B)** NDI1 protein quantification in whole brain tissue using a Wes automated capillary-based fluorescent immunoassay system. The area of fluorescent peaks detected at 58 kDa (predicted NDI1 molecular weight) divided by the area of peaks detected at 111 kDa (predicted Vinculin molecular weight) as a loading control were used to generate bar graphs of relative protein abundance of NDI1 at 7 weeks of age and at greater than 6 months of age to demonstrate that NDI1 protein remains detectable in adult brain tissue. **(C)** NDUFS4 protein quantification in whole brain tissue using a Wes automated capillary-based fluorescent immunoassay system. The area of fluorescent peaks detected at 26 kDa (predicted NDUFS4 molecular weight) divided by the area of peaks detected at 52 kDa (predicted Tubulin molecular weight) as a loading control were used to generate bar graphs of relative protein abundance of NDUFS4 at 7 weeks of age and at greater than 6 months of age to demonstrate appropriate depletion of NDUFS4 gene in adult brain tissue. **(D)** NDI1 and **(E)** NDUFS4 mRNA measured by qPCR from astrocytes and microglia were sorted from adult NDI1 expressing mice and NDUFS4 cKO mice to confirm appropriate recombination by Nestin Cre in neural lineage cells (astrocytes) but not microglia. **(F)** Sort layout and gating strategy for mRNA analysis of astrocytes and microglia. **(G)** DropViz data suggests that in the mouse cerebellum the relative NDUFS4 expression is highest in cerebellar granule neurons. Publicly available Drop-seq data on the DropViz online platform was used to query NDUFS4 expression by putative cell type cluster in the mouse cerebellum.

Figure S2, Related to Figure 2 Characterization of persistently ataxic cKO+NDI1 muscle. **(A)** Representative Hematoxylin and Eosin (H&E) and **(B)** trichrome staining of quadriceps cross section in both NDI1 control and cKO + NDI1 ataxic mice over 1 year of age. No central nuclei or ragged-red-fibers are observed. **(C)** Quantification of relative mean fiber diameter in quadriceps muscle (N=6 per genotype, T-test not significant). **(D)** Quantification of NDUFS4 protein abundance in quadriceps muscle using a Wes automated capillary-based fluorescent immunoassay system. The area of fluorescent peaks detected at 26 kDa (predicted NDUFS4 molecular weight) divided by the area of peaks detected at 52 kDa (predicted Tubulin molecular weight) as a loading control were used to generate bar graphs of relative protein abundance of NDUFS4 at over 1 year of age (N=6 per genotype, T-test not significant). **(E-G)** Soluble metabolite measurements of quadriceps muscles at over 1 year of age. **(E)** Multiple T-tests with multiple hypothesis adjustment to 0.1 resulted in no discoveries of significantly different metabolite levels (N=6 per genotype). **(F)** Principal component analysis scores plot of muscle metabolite profile. **(G)** Heatmap of top 25 candidate metabolites ranked by T-test P-value Z-scores calculated by row.

Figure S3, Related to Figure 3. Representative histology images demonstrate microglial and astrocyte activation in the brain stem, olfactory bulb, and cerebellum, and representative whole-body plethysmography tracings. **(A)** Representative whole-body plethysmography breathing patterns of cKO+NDI1 (left) and cKO (right) mice at over 7 weeks of age with times of regular and irregular breathing patterns in both groups. No apneas were observed in either group. **(B)** DAB staining of IBA1 for microglial abundance and morphology as an indicator of neuroinflammation. 63x representative images of mouse olfactory bulb, brainstem, and cerebellum cut in horizontal section. **(C)** DAB staining of GFAP for astrocyte abundance and activation morphology as an indicator of neuroinflammation. 40x representative images of mouse olfactory bulb, brainstem, and cerebellum cut in horizontal section.

Figure S4,related to Figure 4. Metabolic characterization of primary glia and RNA-seq data. **(A)** Uniformly labeled 13C-glucose metabolite tracing in cultured astrocyte-enriched primary cells from early post-natal mice for 6 hours. The percentage of the total pool was calculated for each condition (N=3-7 per group, * indicates significant two-way-ANOVA $P<0.05$ with Tukey's multiple comparisons test vs WT adjusted $P<0.05$ for M+0 peak, ANOVAs calculated independently for each metabolite). **(B)** Mitochondrial complex I-dependent ADP stimulated respiration in permeabilized astrocyte-enriched primary brain cultures. Cells were permeabilized and provided the complex I substrates pyruvate and malate. (N=3-7 per group, ANOVA not significant). **(C)** Mitochondrial complex II-dependent ADP-stimulated respiration in permeabilized astrocyte-enriched primary brain cultures. Cells were permeabilized and provided the complex II substrate succinate along with ADP and complex I inhibitors. (N=3-7 per group, ANOVA not significant). **(D)** NADH/NAD+ ratio in cultured astrocyte-enriched primary cells from early post-natal WT vs NDI1 expressing mice. NDI1 expression prevents a significant increase in the NADH/NAD+ ratio following mitochondrial complex I inhibition with Piericidin A. (N=3 per group, * indicates one-way ANOVA $P=0.0003$ with Tukey's multiple comparisons tests WT Vehicle vs WT 1μM Piericidin A adjusted $P=0.0003$). **(E)** RNA sequencing analysis of whole cerebellum tissue. Significantly differentially expressed genes between Cre, NDI1, cKO, and cKO+NDI1 samples were determined with a likelihood ratio test using a threshold adjusted P value of 0.05 and then clustered.

Figure S1:

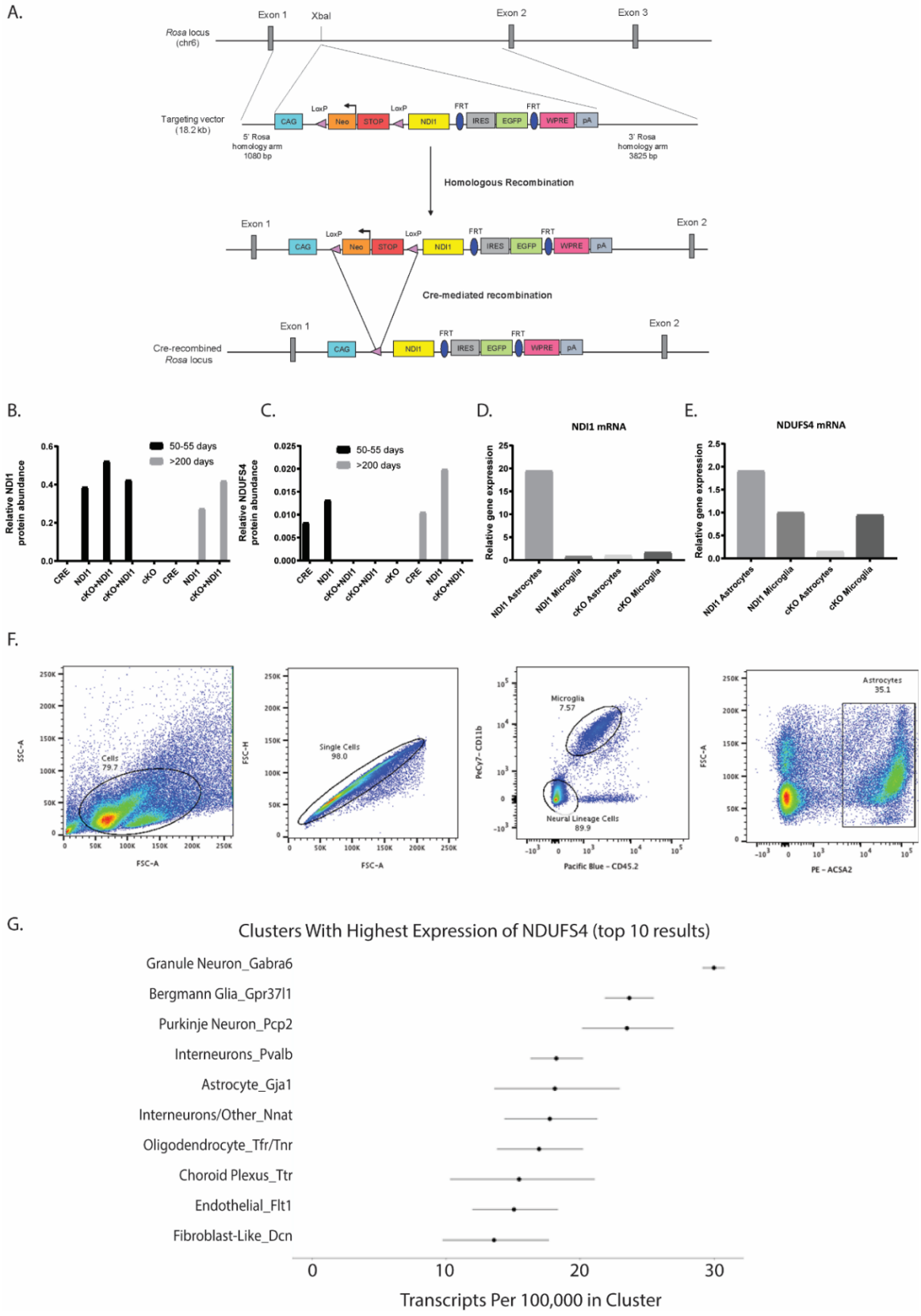
A.
Exon 1
XbaI
Exon 2
Exon 3
Rosa locus (chr6)
Targeting vector (18.2 kb)
CAG
LoxP
Neo
STOP
LoxP
NDI1
FRT
IRES
EGFP
FRT
WPRE
pA
5' Rosa homology arm 1080 bp
3' Rosa homology arm 3825 bp
Homologous Recombination
Cre-mediated recombination
Cre-recombined Rosa locus
B.
Relative NDI1 protein abundance
50-55 days
>200 days
CRE
NDI1
cKO+NDI1
cKO
C.
Relative NDUFS4 protein abundance
D.
NDI1 mRNA
Relative gene expression
NDI1 Astrocytes
NDI1 Microglia
cKO Astrocytes
cKO Microglia
E.
NDUFS4 mRNA
F.
SSC-A
FSC-A
Cells 79.7
FSC-H
Single Cells 98.0
PeCy7 - CD11b
Pacific Blue - CD45.2
Microglia 7.57
Neural Lineage Cells 89.9
Astrocytes 35.1
PE - ACSA2
G.
Clusters With Highest Expression of NDUFS4 (top 10 results)
Granule Neuron_Gabra6
Bergmann Glia_Gpr37l1
Purkinje Neuron_Pcp2
Interneurons_Pvalb
Astrocyte_Gja1
Interneurons/Other_Nnat
Oligodendrocyte_Tfr/Tnr
Choroid Plexus_Ttr
Endothelial_Flt1
Fibroblast-Like_Dcn
Transcripts Per 100,000 in Cluster

Figure S2:

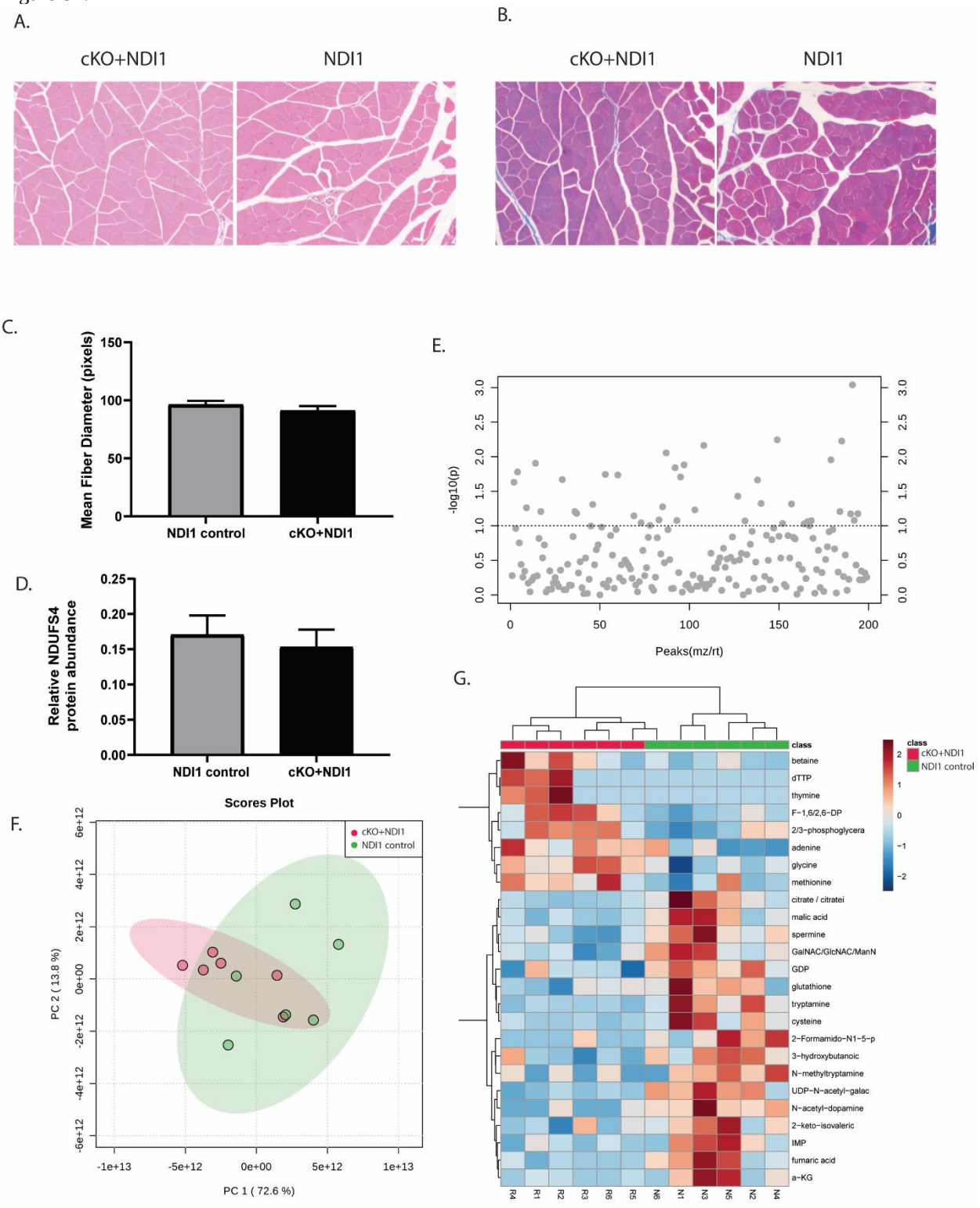
A.
cKO+NDI1
NDI1
B.
cKO+NDI1
NDI1
C.
Mean Fiber Diameter (pixels)
150
100
50
0
NDI1 control
cKO+NDI1
D.
Relative NDUFS4 protein abundance
0.25
0.20
0.15
0.10
0.05
0.00
NDI1 control
cKO+NDI1
E.
-log10(p)
Peaks(mz/rt)
F.
Scores Plot
cKO+NDI1
NDI1 control
PC 2 (13.8 %)
PC 1 (72.6 %)
G.
class
cKO+NDI1
NDI1 control
betaine
dTTP
thymine
F−1,6/2,6−DP
2/3−phosphoglycera
adenine
glycine
methionine
citrate / citratei
malic acid
spermine
GalNAC/GlcNAC/ManN
GDP
glutathione
tryptamine
cysteine
2−Formamido−N1−5−p
3−hydroxybutanoic
N−methyltryptamine
UDP−N−acetyl−galac
N−acetyl−dopamine
2−keto−isovaleric
IMP
fumaric acid
a−KG

Figure S3:

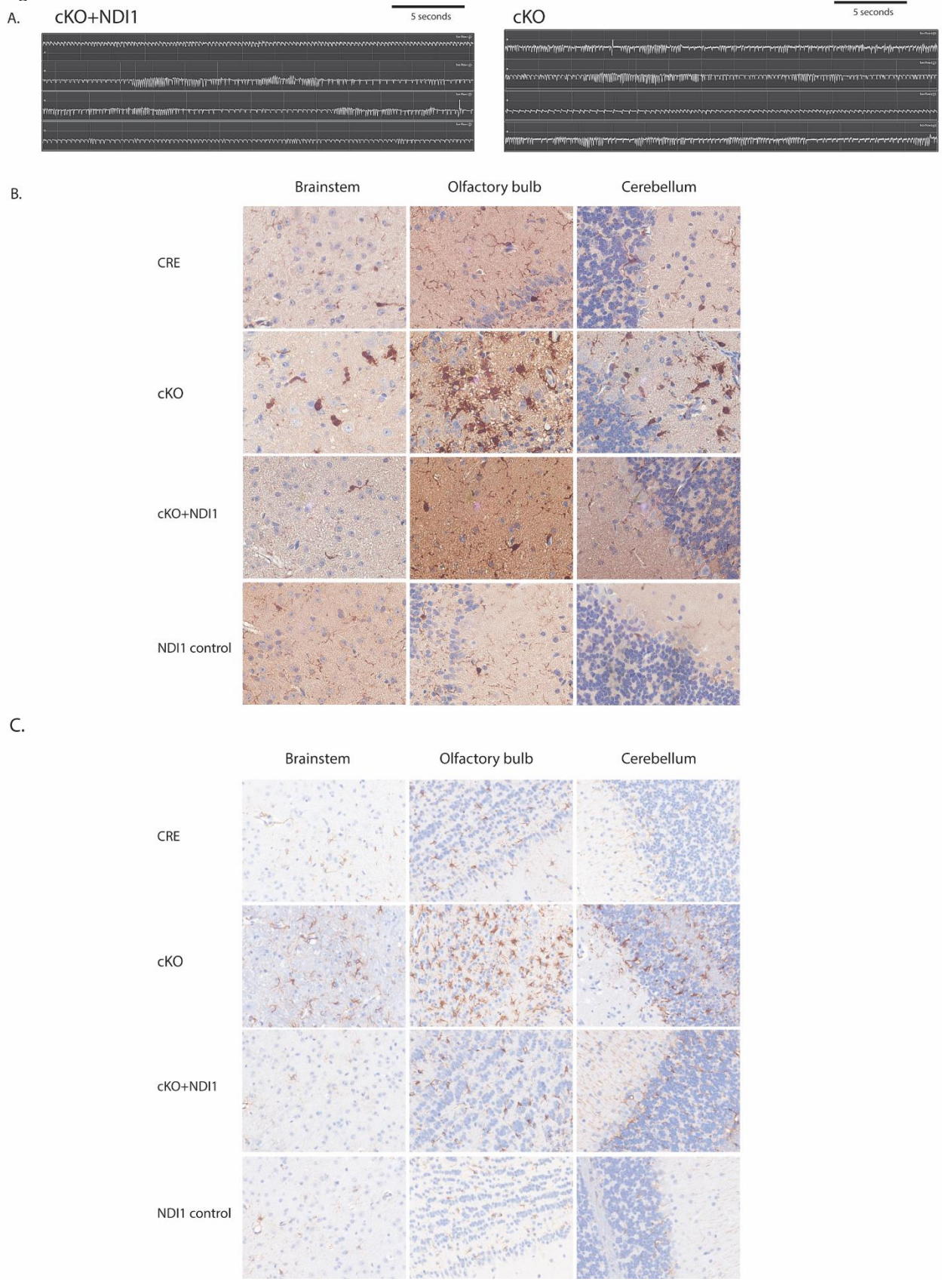
A.
cKO+NDI1
5 seconds
cKO
5 seconds
B.
Brainstem
Olfactory bulb
Cerebellum
CRE
cKO
cKO+NDI1
NDI1 control
C.
Brainstem
Olfactory bulb
Cerebellum
CRE
cKO
cKO+NDI1
NDI1 control

Figure S4:

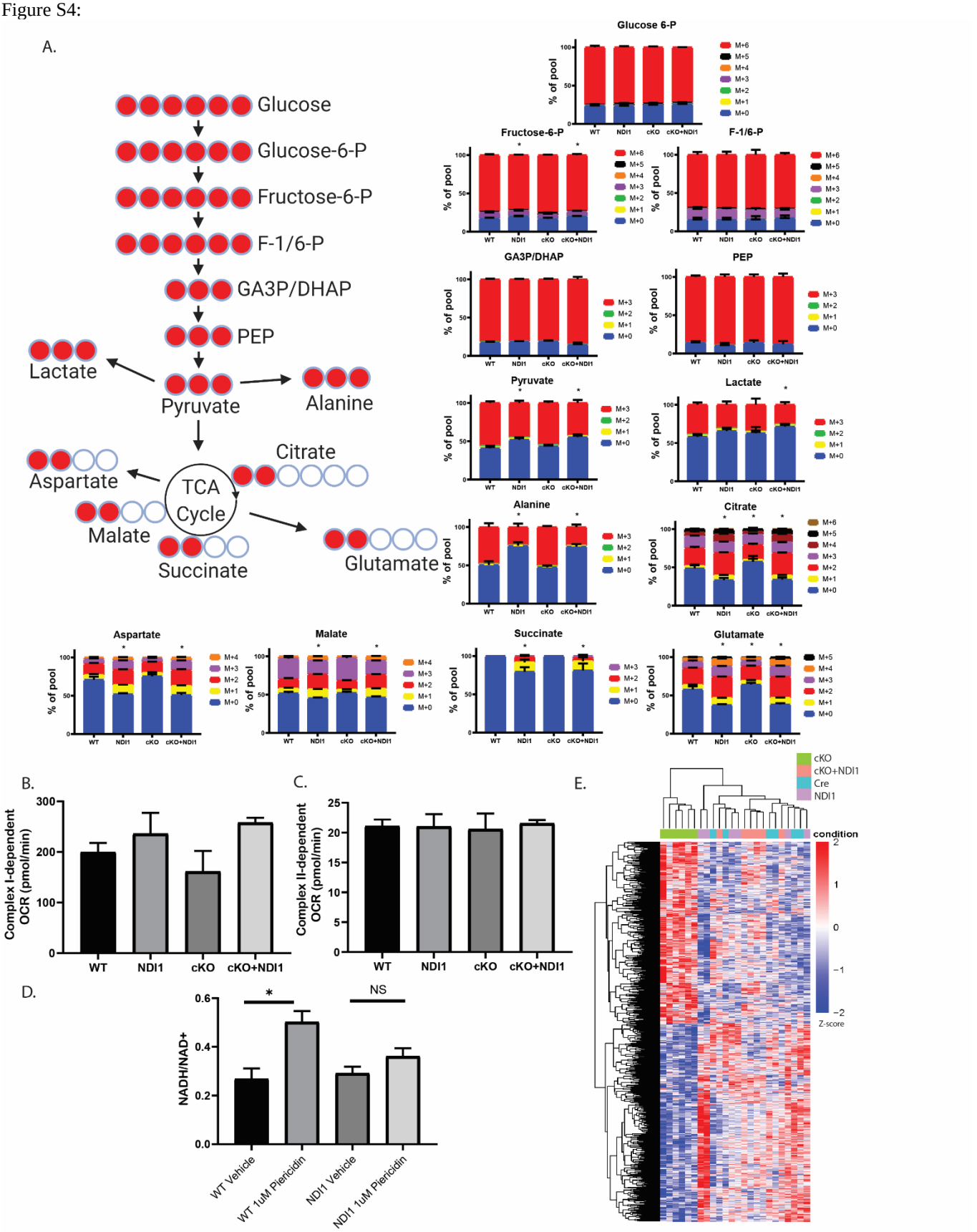
A.
Glucose
Glucose-6-P
Fructose-6-P
F-1/6-P
GA3P/DHAP
PEP
Lactate
Pyruvate
Alanine
Citrate
Aspartate
TCA Cycle
Malate
Succinate
Glutamate
Glucose 6-P
Fructose-6-P
F-1/6-P
GA3P/DHAP
PEP
Pyruvate
Lactate
Alanine
Citrate
Aspartate
Malate
Succinate
Glutamate
% of pool
WT
NDI1
cKO
cKO+NDI1
B.
Complex I-dependent OCR (pmol/min)
C.
Complex II-dependent OCR (pmol/min)
D.
NADH/NAD+
*
NS
WT Vehicle
WT 1uM Piericidin
NDI1 Vehicle
NDI1 1uM Piericidin
E.
cKO
cKO+NDI1
Cre
NDI1
condition
Z-score